applied optics

Off-axis three-mirror freeform telescope with a large linear field of view based on an integration mirror

Qingyu Meng,[1,2,*] Hongyuan Wang,[1] Kejun Wang,[2] Yan Wang,[2] Zhenhua Ji,[2] and Dong Wang[2]

[1]Research Center for Space Optical Engineering, Harbin Institute of Technology, No. 2 Yikuang Street, Harbin 150001, China
[2]Changchun Institute of Optics, Fine Mechanics and Physics, Chinese Academy of Sciences, No. 3888, Dongnanhu Road, Changchun 130033, China
*Corresponding author: mengqy@ciomp.ac.cn

Received 21 July 2016; revised 5 October 2016; accepted 6 October 2016; posted 10 October 2016 (Doc. ID 270881); published 3 November 2016

We report on the design of an off-axis three-mirror freeform telescope with a large field of view (FOV) based on an integration mirror (IM). This design is the continuation of the authors' previous work. Based on aberration theory, we established a suitable nonrelayed three-mirror-anastigmat initial configuration for integration mirror design. For an optical freeform surface, we analyzed the qualitative aberration correction ability of a *x-y* polynomial surface that can provide a simple, convenient, and user-friendly relationship between freeform surface term coefficients and aberrations and then applied the *x-y* polynomial surface on the tertiary mirror to improve the system optimization degrees of freedom. In an example with a focal length of 1200 mm, an F-number of 12, and a FOV of 1° × 30°, the tolerance performance was analyzed, and the system presented a good imaging performance. In addition, the IM structure and opto-mechanics support structure were designed and analyzed. The confirmatory design results showed that the integration of the primary mirror and tertiary mirror can improve opto-mechanical properties judged by multiple criteria. In conclusion, the integration of the primary mirror and tertiary mirror not only offers alignment convenience as described previously but also improves system opto-mechanical properties in multiple perspectives. We believe this large linear FOV system based on IM has broad future applications in the optical remote sensing field.

OCIS codes: (080.4035) Mirror system design; (080.1010) Aberrations (global); (220.4830) Systems design; (350.6090) Space optics; (120.4880) Optomechanics.

http://dx.doi.org/10.1364/AO.55.008962

1. INTRODUCTION

Reflective optical systems are widely used in the optical remote sensing field because of the characteristics of good thermal performance, wide working spectrum range, etc. Off-axis reflective optical systems evolved from coaxial reflective optical systems are getting more and more attention due to the advantages of much wider field of view (FOV), better spot diagram energy concentration, and improved observation frequency of specified target areas [1,2], despite some drawbacks in the off-axis system, such as alignment difficulties and high manufacturing costs. In recent decades, off-axis reflective optical systems have been applied in a large number of well-known astronomical telescopes, such as SPOT-5, QuickBird, ALOS-3, and CARTOSAT-1 [2–4].

Push-broom imaging is a frequently applied mode of optical remote sensing in ground sampling. Improving temporal resolution and getting a wide area at a time is always a desire of consumers. Increasing the FOV is a simple and reliable approach to improve temporal resolution. However, the off-axis reflective optical system with simple surface types has fewer designs and optimization degrees of freedom (DOFs), so it is challenging to achieve a very large FOV capable of obtaining a wide imaging swath.

In early years of optical system designing and manufacturing, almost only spherical surfaces were applied in the optical system. Then with the development of the computer-based calculation and optical surface manufacturing technology, aspheric surfaces have become the solution of choice in modern high-end optics [5]. In past two decades, due to the rapid development of aberration theory, optical system optimization techniques, computational speed, fabrication precision of surfaces without symmetry, and extensions of the range of the surface slopes allowed in optical testing, all of which allowed optical freeform surfaces [6], offer more DOFs and present stronger abilities in aberration correction. Such improvements in optical freeform surfaces have been successfully applied in

illumination and imaging systems by providing better imaging quality, a wider FOV, a faster F-number, and so on.

This paper mainly focus on the integration of the primary mirror (PM) and tertiary mirror (TM) [1] of the large linear FOV three-mirror-anastigmat (TMA) system and its main content involving optical system design, qualitative aberration relationship analysis, and opto-mechanics confirmatory design. An off-axis three-mirror freeform system with a large linear FOV based on an integration mirror (IM) is achieved. The paper's contribution mainly concentrates on the following parts.

First, based on third-order aberration theory, the design principles are illustrated, and from the points of optical system configuration and mirror configuration opto-mechanical layout, the optical system configuration restriction condition more suitable for engineering is established.

Second, qualitative aberration correction ability of the *x-y* polynomial surface is analyzed. Then the *x-y* polynomial surface is used in the optical system design. During the optical system design process, the qualitative analysis results can be used to guide computer-aided design software to adjust and optimize the freeform parameters. It helps us in designing a fine-imaging quality system with a FOV of 30° × 1°, and the system performance has better progress than we have done before. The design results prove that our method is effective in optical system design, the method is easy to use, and it also helps us understand the aberration correction ability of the freeform surface easily.

Third, a design example with a focal length of 1200 mm, an *F*-number of 12, and a large FOV of 1° × 30° is given. The system has good performance and symmetrical imaging quality on the tangential plane. For the integration of the PM and TM, tolerances including manufacturing tolerance, integration manufacturing tolerance, and alignment tolerance are analyzed.

Finally, for opto-mechanical performance, we verify the superiority of the integration of the PM and TM. By confirmatory opto-mechanical design, we learn that the integration of the PM and TM not only offers alignment convenience but also improves opto-mechanics properties in multiple perspectives, such as mirror statics surface shape and the mirror light–weight ratio.

Upon comprehensive analysis, we believe this large linear FOV system based on IM will have broad applications in the optical remote sensing field.

2. DESIGN PRINCIPLE AND ESTABLISHING INITIAL CONFIGURATION BASED ON THIRD-ORDER ABERRATION

A. Mirror Configuration Opto-Mechanical Layout Analysis

There are two types of widely used optical remote sensor of off-axis TMA optical systems [7]: relayed TMA [8] and nonrelayed TMA [9,10], as shown in Figs. 1 and 2, respectively.

In a relayed TMA system, aperture stop is usually located at the front of the system, and sometimes the aperture stop is also set as the entrance pupil. The system has the characteristics of compact size and a high telephoto ratio. The QuickBird telescope is an example of a relayed TMA system, which achieves a FOV of 2.1°, a focal length of 9 m, and an *F*-number of 15 [3,11]. In a relayed TMA system, there is an intermediate image plane between the secondary mirror (SM) and the TM, and this position is suitable for laying a rear stop to suppress stray light. However, because the aperture stop is at the front of the optical system, which makes the system asymmetric, the relayed TMA system cannot achieve a wide FOV.

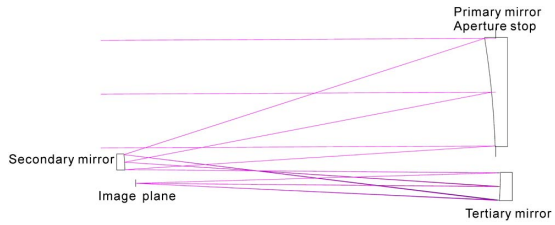

Fig. 1. Relayed TMA optical system.

Fig. 2. Nonrelayed TMA optical system.

By contrast, in a nonrelayed TMA system, the SM is set as the aperture stop, so the PM and TM are symmetrical relative to the SM. This characteristic is conducive to lateral aberration correction, which is analogous to the Cooke triplet, so this optical configuration is capable of achieving a large Lagrange invariant and a wide FOV. The PM and the TM are on both sides of the aperture stop (SM); the PM and TM surface ranges are the projections of the subentrance pupil of each FOV, so the PM and TM sizes are very large in a wide FOV system.

For a push-broom imaging mode optical remote sensor, when we want to obtain a large swath image by a large linear FOV nonrelayed TMA system, the PM and TM overall dimensions will be rectangular with a high aspect ratio (AR) [12].

For space applications, mirror light–weight is an important index. A circular mirror or a square mirror manufactured by silicon carbide (SiC) or low-expansion quartz glass can achieve very fine surface shape error in a large diameter–thickness ratio (DTR), where the value can usually approach 15 in well-designed support structures. However, a large AR rectangular mirror usually cannot achieve an outstanding DTR with a fine surface shape error with the same mechanical properties as a circular mirror or a square mirror.

In our previous work, an off-axis TMA system with wide FOV based on the integration of the PM and TM was designed for the purpose of extending optimization freedom, decreasing alignment freedom, and reducing alignment difficulty. Now, for further application requirements, we aim to design an off-axis nonrelayed TMA freeform telescope with a large linear FOV in which the PM and TM are two rectangular mirrors with high AR, respectively. In the process of optical system

design, we also decided to manufacture the PM and TM in one single substrate in order to achieve the following benefits.

First, the application of an optical freeform surface can extend the system design freedom; thus, a high-performance TMA optical system will be obtained.

Second, we will get the same result as the previous work, where the optical system alignment DOFs will be decreased, and the alignment difficulty will also be reduced.

Third, and most importantly, with two large AR mirrors integrated in a single substrate, the IM's AR will be smaller, and the DTR can be designed larger in the same magnitude order of mirror shape error performance, and in theory the mirror light–weight ratio also can be improved. Furthermore, the IM will only need one set of opto-mechanical structures rather than two separated mirrors, so the opto-mechanical structure will be simpler.

In summary, the IM design philosophy can improve optical and opto-mechanical properties in multiple perspectives.

B. Design Principle and Establishing Initial Configuration Based on Third-Order Aberration

We have reported that there are four parameters α_1, α_2, β_1, and β_2 determining the TMA configuration. α_1, α_2, β_1, and β_2 are the PM obscuration ratio caused by the SM, the SM obscuration ratio caused by the TM, the SM magnification, and the TM magnification, respectively. They have relationships with r_1, r_2, r_3, d_1, and d_2, which are the PM radius of curvature, the SM radius of curvature, the TM radius of curvature, the distance between the PM and the SM, and the distance between the SM and the TM, respectively. We also can obtain third Seidel aberration from α_1, α_2, β_1, and β_2.

In the previous work, in order to fabricate the PM and TM on a single substrate easily so as to achieve the mirror integration, we restrict the PM and TM as having the same axial position, the same radius of curvature, and the same conical coefficient, i.e., $k_1 = k_3$. From the standpoint of mirror manufacturability, our original intention was to make the PM and TM aspherical grinding together and to reduce the milling cutter repetitive position error to obtain high positional accuracy. To some extent, these actions limit system optimization DOFs, restrain optical system focal power distribution, and impact optical system performance. Learning from the literature [13–16], we noticed two mirrors that have different radii of curvature and conical coefficients can also be manufactured on a single substrate and obtain high positional accuracy. In our following work, we release a design limit in the initial configuration establishing process and from the standpoint of engineering realizability and rationality. In order to obtain a set of suitable configuration parameters, we also apply some additional restrictions as the follows:

(i) In reality, the PM and TM axial position minor differences have little influence on the two mirrors' integration realizability. Therefore, for the convenience of calculation, we restrict the PM and TM to have the same axial position, $d1 = -d2$. Thus, we have

$$\frac{1-\alpha_1}{\alpha_1} = \beta_1(\alpha_2 - 1). \tag{1}$$

(ii) In the following design, a freeform surface is applied to release system optimization in the DOFs. In order to reduce optical system complexity, the SM surface type is to be designed by a spherical mirror, so the SM conical coefficient $k_2 = 0$.

(iii) To restrict overall system length, we request the imaging distance (back focal length) is no greater than twice the distance between the PM and the SM (d_1), so there is the following relationship:

$$\alpha_1\alpha_2 \geq 2\frac{1-\alpha_1}{\beta_1\beta_2}, \tag{2}$$

$$\beta_2 \leq 2 - \frac{2}{\alpha_2}. \tag{3}$$

By Eq. (2), $\alpha_1\alpha_2$ is the system imaging distance, $(1-\alpha_1)/\beta_1\beta_2$ is d_1, and then we can get Eq. (3) from Eq. (2).

(iv) Smaller SM obscuration can bring convenience for an off-axis TMA establishment by means of adding smaller off-axis magnitude on a coaxial TMA, so we make the restriction that α_1 is not greater than 0.5:

$$\alpha_1 \leq 0.5. \tag{4}$$

(v) Furthermore, to restrict the TM diameter, we define the following β_1 and β_2 restrictions:

$$\beta_1 \geq 8, \qquad \beta_2 \leq 0.3. \tag{5}$$

Based on above restriction condition, we solve aberration Eq. (6) for the optimal solution by the least squares method. It is important to note that because we restrict the PM and TM to have the same axial position, only three variables of "α_1, α_2, β_1, and β_2" have been retained. In order to obtain the aberration Eq. (6) unique solution, only three types of aberrations S_I, S_{II}, and S_{III} are considered, and other types of aberration will be balanced during system design process. We have

$$\begin{bmatrix} S_I \\ S_{II} \\ S_{III} \end{bmatrix} = \begin{bmatrix} A_1(\beta_1,\beta_2) & B_1(\beta_1,\beta_2) & C_1(\alpha_1,\alpha_2,\beta_2) \\ A_2(0) & B_2(\alpha_1,\beta_1,\beta_2) & C_2(\alpha_1,\alpha_2,\beta_1,\beta_2) \\ A_3(0) & B_3(\alpha_1,\beta_1,\beta_2) & C_3(\alpha_1,\alpha_2,\beta_1,\beta_2) \end{bmatrix} \times \begin{bmatrix} -k_1 \\ 0 \\ -k_3 \end{bmatrix} + \begin{bmatrix} D_1(\alpha_1,\alpha_2,\beta_1,\beta_2) \\ D_2(\alpha_1,\alpha_2,\beta_1,\beta_2) \\ D_3(\alpha_1,\alpha_2,\beta_1,\beta_2) \end{bmatrix} = \begin{bmatrix} 0 \\ 0 \\ 0 \end{bmatrix}. \tag{6}$$

In Eq. (6) Ai, Bi, Ci, and Di ($I = 1, 2, 3$) are functions of α_1, α_2, β_1, and β_2. We will get a series of solutions in the domain of definition of α_1, α_2, β_1, and β_2. Furthermore, we get the TMA configuration parameters r_1, r_2, r_3, d_1, d_2, and k_1, k_2.

3. ANALYSIS OF THE FREEFORM SURFACE ABERRATION RELATIONSHIP

Freeform surface [17] is a category of nonrotational symmetric surfaces, and they have strong aberration correction ability realized by their multi-DOFs rather than conventional optical surfaces. Now, due to the high imaging quality requirement, freeform surfaces are applied in some telescopes successfully, such as the EAS program IRLS [18] and the UK Astronomy Technology Center program SCUBA-2 [19]. Some recent research reports show us that freeform has the needed performance

to achieve a high-quality optical system: Hou *et al.* has designed short-focal-length off-axis freeform imaging systems with ultra-wide linear FOVs of 70° in the optical tangential direction whose major difference from our following system is that the large FOV is in the sagittal direction [20]. Yang *et al.* has designed a compact freeform infrared TMA system with a rectangle FOV of 4° × 3° [21]. McGuire, Jr. from NASA's Jet Propulsion Laboratory has designed an $f/2.5$, four-mirror telecentric telescope with a FOV of 8.5° × 25.5° using a freeform surface with good results [22].

Zernike polynomial, *x-y* polynomial (extended polynomials in x, y), and extended spline polynomial are representative types of freeform surfaces description. Among them, the *x-y* polynomial, a classical nonorthogonal monomial representation, which coincides with the description of numerical control (NC) optical manufacturing and is fit to machine certain expressions [23], is widely used. In CODE V, the *x-y* polynomial surface is a tenth-order polynomial surface added to a base conic. The polynomial is expanded into monomials of $x^m y^n$, where $m + n \le 10$ [24]. The equation used is

$$z = \frac{cr^2}{1 + \sqrt{1 - (1 + k)c^2 r^2}} + \sum_{j=2}^{66} C_j x^m y^n, \tag{7}$$

where z is the sag of the surface parallel to the z-axis, c is the vertex curvature, k is the conic constant, and C_j is the coefficient of the monomial $x^m y^n$.

Using a smaller number of aspherical terms to correct the system wavefront error (WFE) is the aspheric surface application principle. It is essential to analyze the relationship between freeform surface term coefficients and aberrations. Atchison has given out the explicit quantitative aberration relationship between Taylor polynomial coefficients and Zernike polynomial coefficients [25]. In this paper, a qualitative method is used to describe the relationship between freeform surface term coefficients and aberrations. The analysis can contribute as a guide in our TMA optical system design. Although this method is qualitative, it will provide a simple, convenient, and user-friendly relationship between freeform surface term coefficients and aberrations.

It is well known that, in the optical system design process, one type negative aberration can balance out positive aberration of the same type, and this performance illustrates that one type of surface can balance out the same kind of aberration generated in the overwhelming majority of cases. Now we establish a simple ideal one-mirror system (with an aperture diameter of 50 mm and a wavelength of 632 nm) by means of adding a freeform surface term on the surface, observing which type of aberration is generated in the image field, and based on this qualitative method evaluate the corresponding relationship between freeform surface term coefficients and aberrations. To prevent the impact of off-axis aberration, only axial FOV (0° FOV) is applied in the one-mirror system. Furthermore, the mirror surface is set as a paraboloid ($k = -1$) to prevent the impact of spherical aberration. Here, only primary aberration is analyzed. The aberration performance is shown in Table 1, where each row represents the freeform surface term coefficients (in lens units) and the single-mirror system wavefront Zernike aberrations (in wavelength units) derived by the coefficients.

From Table 1, we can obtain the qualitative aberration correction ability of the *x-y* polynomial surface as follows:

(i) When the x power and the y power are odd, the surface can correct astigmatism (axis at ±45°).

(ii) When the x power is odd and the y power is even, the surface can correct distortion tilt (x-axis) and coma (x-axis); when the x power is even and the y power is odd, the surface can correct distortion tilt (y-axis) and coma (y-axis). In the above conditions, exchange the power of x and y with each other and the surface generates an equal amount of aberration, but the aberration direction is changed.

(iii) When the x power and the y power are different but are all even, the surface can correct field curvature, astigmatism (axis at 0° or 90°), and spherical aberration. When the x power and the y power are the same even number, the surface can correct field curvature and spherical aberration. In the above conditions, exchange the power of x and y with each other and only the astigmatism (axis at 0° or 90°) sign is reversed.

Besides, each freeform term of the *x-y* polynomial surface can also generate other types of primary aberration, but the magnitude is relatively small and the pattern is not obvious.

From the above analysis, we obtain the relationship between the *x-y* polynomial surface and aberration, and then we use the freeform surface to design our system and use the qualitative analysis results to guide CODE V by adjusting and optimizing the freeform parameters. In the design process, as mentioned in our previous work, only even order terms of x are retained in the *x-y* polynomial to keep the system symmetric imaging quality.

4. DESIGN EXAMPLE

A. Optical System Design

Based on the analysis of the previous sections, a nonrelayed TMA initial configuration shown in Fig. 3 is obtained with $\alpha_1 = 0.5$, $\alpha_2 = 2$, and $\beta_1 = \beta_2 = 1$ from Eqs. (1–6). The initial configuration only has one FOV point (0°, 3°).

The off-axis system has a focal length of 1200 mm, an F-number of 12, and an off-axis FOV of −3.5°. The system has a linear FOV of 1° × 30°, the tangential direction (y direction) FOV is 1°, where the range is from −3° to −4°, and the sagittal direction (x direction) FOV is 30°, where the range is from −15° to 15°.

The modulation transfer function (MTF) of initial the configuration is shown in Fig. 4. The MTF has good performance in all spatial frequencies.

In order to achieve our design targets, obtaining a large linear FOV TMA system, freeform surface is applied in the optical system, and the optimization process is achieved with optical design software CODE V.

We set $d_1 = -d_2$ as the boundary condition, and the PM, SM, and TM surface types are set as even asphere, sphere, and *x-y* polynomial, respectively. During the design process, we distribute and adjust the TM *x-y* polynomial coefficients in the optical system design software under the guidance of Table 1. The system final design result is shown in Fig. 5.

Table 1. Aberration Performance

					Fringe Zernike Item (λ, λ = 632.8 nm)								
					1	2	3	4	5	6	7	8	9
No.	Item	x Power	y Power	Coefficient (mm)	Piston	Tilt-x	Tilt-y	defocus	Astig-0°	Astig-45°	Coma-x	Coma-y	Spherical
1	X^1Y^0	1	0	1e-5	0	0	0	0	0	0	0	0	0
2	X^0Y^1	0	1	1e-5	0	0	0	0	0	0	0	0	0
3	X^2Y^0	2	0	1e-5	−4.9386	0	0	−4.9356	−9.8757	0	0	0	0.0030
4	X^1Y^1	1	1	1e-5	−0.0001	0	0	−0.0001	0	−9.8752	0	0	0
5	X^0Y^2	0	2	1e-5	−4.9386	0	0	−4.9356	9.8757	0	0	0	0.0030
6	X^3Y^0	3	0	1e-7	0	−2.4692	0	0	0	0	−1.2332	0	0
7	X^2Y^1	2	1	1e-7	0	0	−0.8231	0	0	0	0	−0.4111	0
8	X^1Y^2	1	2	1e-7	0	−0.8231	0	0	0	0	−0.4111	0	0
9	X^0Y^3	0	3	1e-7	0	0	−2.4692	0	0	0	0	−1.2332	0
10	X^4Y^0	4	0	1e-9	−0.1543	0	0	−0.2313	−0.4624	0	0	0	−0.0767
11	X^3Y^1	3	1	1e-9	0	0	0	0	0	−0.2313	0	0	0
12	X^2Y^2	2	2	1e-9	−0.0515	0	0	−0.0773	0	0	0	0	−0.0259
13	X^1Y^3	1	3	1e-9	0	0	0	0	0	−0.2315	0	0	0
14	X^0Y^4	0	4	1e-9	−0.1543	0	0	−0.2314	0.463	0	0	0	−0.077
15	X^5Y^0	5	0	1e-9	−0.0006	−9.6498	0	−0.0014	−0.0026	0	−7.7141	0	−0.0011
16	X^4Y^1	4	1	1e-9	−0.0001	0	−1.9293	−0.0002	−0.0002	0	0	−1.5423	−0.0001
17	X^3Y^2	3	2	1e-9	0	−1.9293	0	−0.0001	0	0	−1.5423	0	−0.0001
18	X^2Y^3	2	3	1e-9	0	0	−1.9293	−0.0001	0	0	0	−1.5423	−0.0001
19	X^1Y^4	1	4	1e-9	−0.0001	−1.9293	0	−0.0002	0.0002	0	−1.5423	0	−0.0001
20	X^0Y^5	0	5	1e-9	−0.0006	0	−9.6498	−0.0014	0.0026	0	0	−7.7141	−0.0011
21	X^6Y^0	6	0	1e-11	−0.603	0	0	−1.085	−2.1697	0	0	0	−0.6022
22	X^5Y^1	5	1	1e-11	0	0	0	0	0	−0.7237	0	0	0
23	X^4Y^2	4	2	1e-11	−0.1206	0	0	−0.217	−0.1455	0	0	0	−0.1204
24	X^3Y^3	3	3	1e-11	0	0	0	0	0	−0.4338	0	0	0
25	X^2Y^4	2	4	1e-11	−0.1206	0	0	−0.217	0.1455	0	0	0	−0.1204
26	X^1Y^5	1	5	1e-11	0	0	0	0	0	−0.7237	0	0	0
27	X^0Y^6	0	6	1e-11	−0.603	0	0	−1.085	2.1697	0	0	0	−0.6022

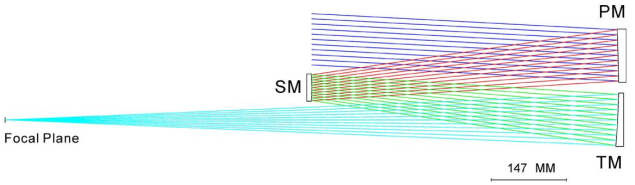

Fig. 3. Initial configuration.

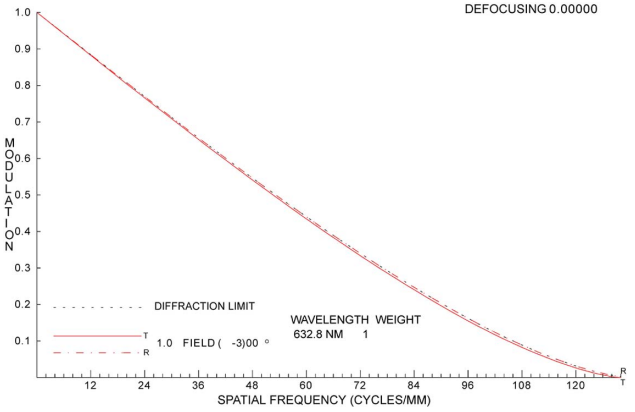

Fig. 4. Initial configuration MTF.

The off-axis TMA system has good imaging quality; the WFE value is shown in Table 2 and Fig. 6, and the maximum RMS value is 0.0534λ (λ/19, λ = 0.6328 μm). The MTF is close to the diffraction limit at 50 lp/mm (shown in Fig. 7). During the design process, the system distortion value is set as one merit function, and the design results show that the grid distortion maximum absolute value is 2.96 mm, the maximum relative value is less than 0.90%, and the schematic is shown in Fig. 8.

The TMA optical system configuration parameters are shown in Table 3. The PM and TM optical overall dimension are 896 mm × 135 mm and 810 mm × 98 mm, respectively. Their AR attain 6.6 and 8.3, respectively, which are large values. The x-y polynomial coefficients of TM are shown in Table 4. Based on the analysis of the x-y freeform surface aberration relationship, 27 freeform coefficients are used (shown in Table 4) to obtain good imaging performance.

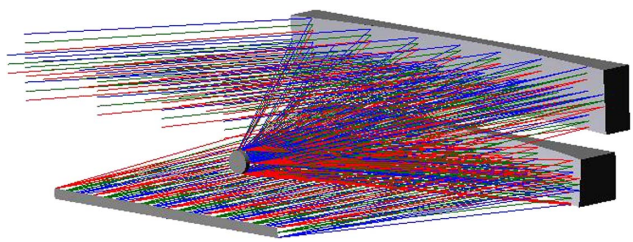

Fig. 5. 3D viewing schematic.

Table 2. WFE Values[a]

X FOV	−15	−10	−5	0
Y FOV	−3	−3	−3	−3
WFE(RMS)	0.0349λ	0.0534λ	0.0445λ	0.0220λ
X FOV	−15	−10	−5	0
Y FOV	−3.5	−3.5	−3.5	−3.5
WFE(RMS)	0.0314λ	0.0300λ	0.0199λ	0.0274λ
X FOV	−15	−10	−5	0
Y FOV	−4	−4	−4	−4
WFE(RMS)	0.0339λ	0.0519λ	0.0520λ	0.0485λ

[a]RMS, $\lambda = 0.6328$ μm.

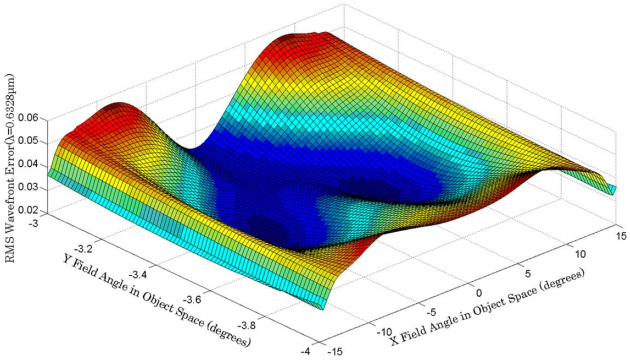

Fig. 6. WFE RMS value ($\lambda = 0.6328$ μm).

Because only even-order terms of x are retained in the x-y polynomial, a symmetrical imaging quality about the tangential plane is obtained, and it can proved by the spot diagram (shown in Fig. 9).

B. Tolerance Analysis

The manufacturing and alignment tolerances have been analyzed with the Monte Carlo method. The tolerance values are shown in Tables 5 and 6. It is necessary to mention that our design goal is to integrate the PM and TM on a single substrate, so during the alignment process the PM and TM have no individual adjustment ability. In turn, this action will bring integration manufacturing tolerances as follows:

(i) Axial distance manufacturing tolerance: one mirror practical axial distance relative to another mirror is inconsistent with the theoretical axial distance [shown in Fig. 10(a)].

(ii) Surface tilt manufacturing tolerance: one mirror surface tilt relative to another mirror [shown in Fig. 10(b)].

(iii) Off-axis amount manufacturing tolerance: one mirror off-axis amount relative to the optical axis is inconsistent with theoretical axial distance [shown in Fig. 10(c)].

(iv) Rotation manufacturing tolerance: one mirror has rotation revolved around its axis [shown in Fig. 10(d)].

During the manufacturing process, some tolerances above are difficult to measure and control. From another point of view, the manufacturing tolerances represent system sensitivity in a certain sense.

Based on the tolerance allocation, the off-axis TMA system has a performance with average WFE RMS $\lambda/12$ (0.0788λ), where the system performance is shown in Table 7. The value is suitable for push-broom remote sensing.

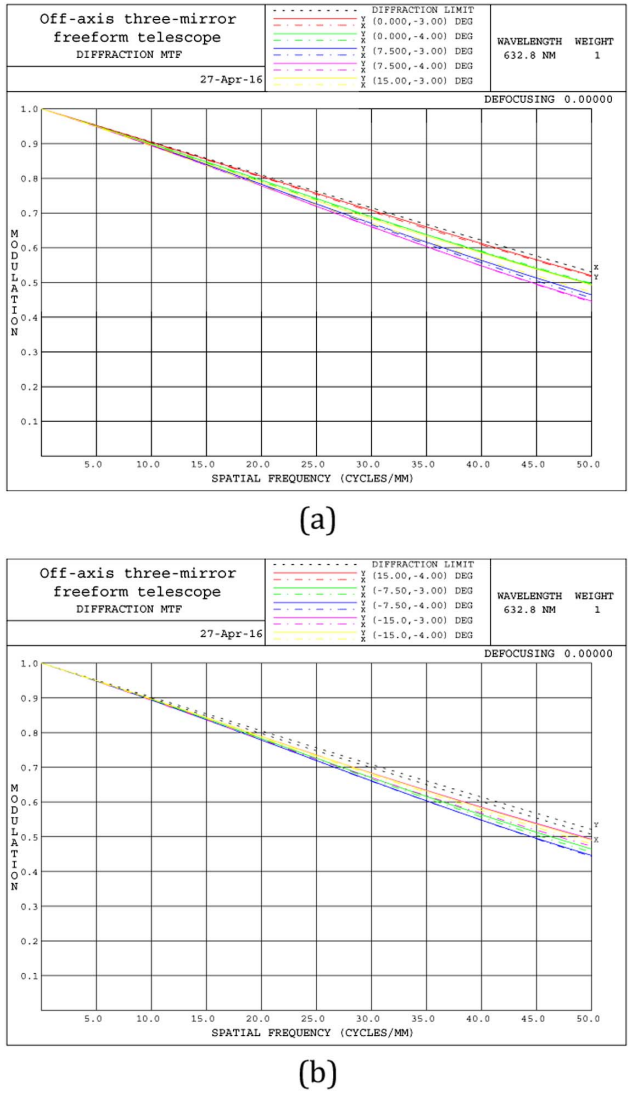

Fig. 7. Modulation transfer function (MTF).

5. OPTO-MECHANICAL SYSTEM DESIGN AND ANALYSIS

In this section, based on the accomplished off-axis TMA system with a large linear FOV, we contrastively analyze the advantages of the integration of the PM and TM from the point of mirror opto-mechanical structure and mirror performance. We have two contrast solutions.

In solution I, the PM and TM are two separated independent mirrors. As shown in Fig. 11, the two mirrors have their

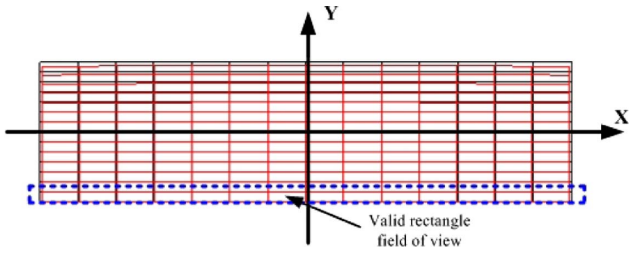

Fig. 8. Grid distortion.

Table 3. Configuration Parameters

	Surface Type	Radius (mm)	Distance (mm)	Conic	High-Order Term 6th	High-Order Term 8th	Mirror Off-Axis Magnitude (mm)	Optical Overall Dimension (mm)
PM	Even Asphere	−2521.85	−645.00	−1.90788	−3.43749e-19	−1.76276e-24	86.5	896 × 135
SM	Sphere	−845.40	645.00	0	—		0	Φ50
TM	X-Y Polynomial	−1208.00	−865.71	0.15601	—		−82	810 × 98

Table 4. Polynomial Parameters of the Freeform TM

No.	Term	Coefficient A_{ij}	No.	Term	Coefficient A_{ij}	No.	Item	Coefficient A_{ij}	No.	Term	Coefficient A_{ij}
1	X^1Y^0	0	8	X^1Y^2	0	15	X^5Y^0	0	22	X^5Y^1	0
2	X^0Y^1	−4.3459e-005	9	X^0Y^3	−9.9726e-009	16	X^4Y^1	9.1916e-016	23	X^4Y^2	8.3213e-019
3	X^2Y^0	−2.3375e-007	10	X^4Y^0	−3.3653e-013	17	X^3Y^2	0	24	X^3Y^3	0
4	X^1Y^1	0	11	X^3Y^1	0	18	X^2Y^3	−1.0668e-015	25	X^2Y^4	−3.4052e-018
5	X^0Y^2	−9.8936e-007	12	X^2Y^2	−2.4520e-012	19	X^1Y^4	0	26	X^1Y^5	0
6	X^3Y^0	0	13	X^1Y^3	0	20	X^0Y^5	−2.2554e-013	27	X^0Y^6	−3.1472e-016
7	X^2Y^1	−5.5852e-010	14	X^0Y^4	−6.6374e-011	21	X^6Y^0	−7.0537e-019			

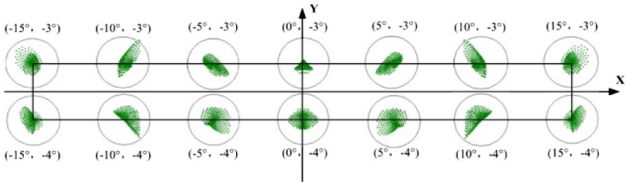

Fig. 9. Spot diagram.

Table 5. Manufacturing Tolerance

	Shape Error RMS (λ)	Δr (mm)	Conic	Integration Manufacturing Tolerance: Off-Axis (mm)	Tilt (″)	Axial Distance (mm)	Rotation (″)
PM	1/50	±2.5	±0.001	±0.5	±30	±2	±10
SM	1/80	±0.8	null	null	null	null	null
TM	1/50	±1.2	±0.0005	±0.5	±30	±2	±10

Table 6. Alignment Tolerance

	Δd	Decenter	Tilt
PM	Reference	Reference	Reference
SM	±2 mm	±0.5 mm	30″
TM	Null	Null	Null

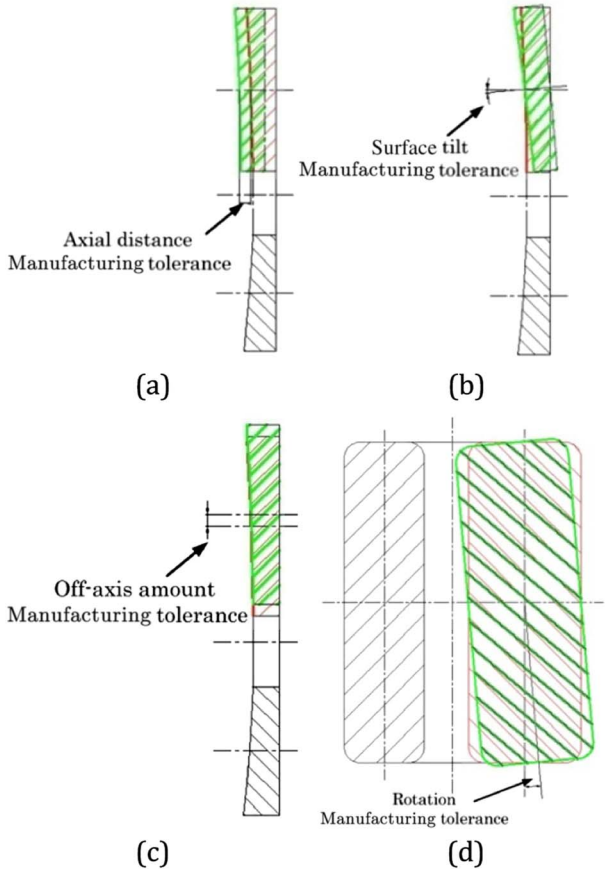

Fig. 10. Diagram showing integration manufacturing tolerances. (a) Axial distance manufacturing tolerance. (b) Surface tilt manufacturing tolerance. (c) Off-axis amount manufacturing tolerance. (d) Rotation manufacturing tolerance.

own support structures, respectively, mainly including an aluminum matrix composite backboard, three sets of invar cone-shaped sheaths, and titanium flexible units, which are the connecting equipment of the mirror and backboard.

In solution II, shown in Fig. 12, based on our design idea, the PM and TM are integrated into one IM, and the IM has only one set of support structures, mainly including one backboard, three sets of cone-shaped sheaths and flexible units.

According to the optimization design, we analyze the two solutions from multiple perspectives.

Table 7. Performance Summary[a]

X FOV	−15	−10	−5	0
Y FOV	−3	−3	−3	−3
Design	0.0349λ	0.0534λ	0.0445λ	0.0220λ
Design and TOL	0.0843λ	0.1000λ	0.0852λ	0.0635λ
X FOV	−15	−10	−5	0
Y FOV	−3.5	−3.5	−3.5	−3.5
Design	0.0314λ	0.0300λ	0.0199λ	0.0274λ
Design and TOL	0.0674λ	0.0638λ	0.0585λ	0.0621λ
X FOV	−15	−10	−5	0
Y FOV	−4	−4	−4	−4
Design	0.0339λ	0.0519λ	0.0520λ	0.0485λ
Design and TOL	0.0908λ	0.0972λ	0.0908λ	0.0818λ

[a]RMS, $\lambda = 0.6328$ μm.

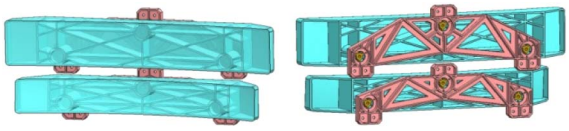

(a) (b)

Fig. 11. Solution I: independent mirrors and support structure. (a) Front and (b) back.

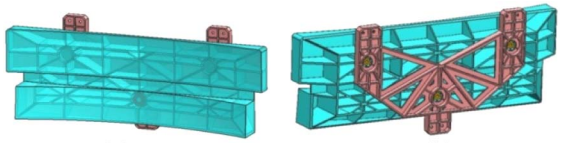

(a) (b)

Fig. 12. Solution II: integration mirror and support structure. (a) Front and (b) back.

From the point of mirror performance, in solution I, the PM and TM sizes are 907 mm × 147 mm and 822 mm × 110 mm, respectively, and the AR values are 6.17 and 7.47, respectively. In solution II, the IM size is 908 mm × 297 mm, and the AR value is 3.06. The smaller AR value in solution II is conducive to achieving a better mirror mechanical property. Although the mirror thickness is 70 mm in both solutions, the IM's DTR value (13.64) is larger in solution II than in solution I. With respect to light–weight performance, in solution I, the PM and TM light–weight ratios achieve 71.2% and 74.6%, and in solution II, the IM light–weight ratio achieves 78.9%, as shown in Table 8.

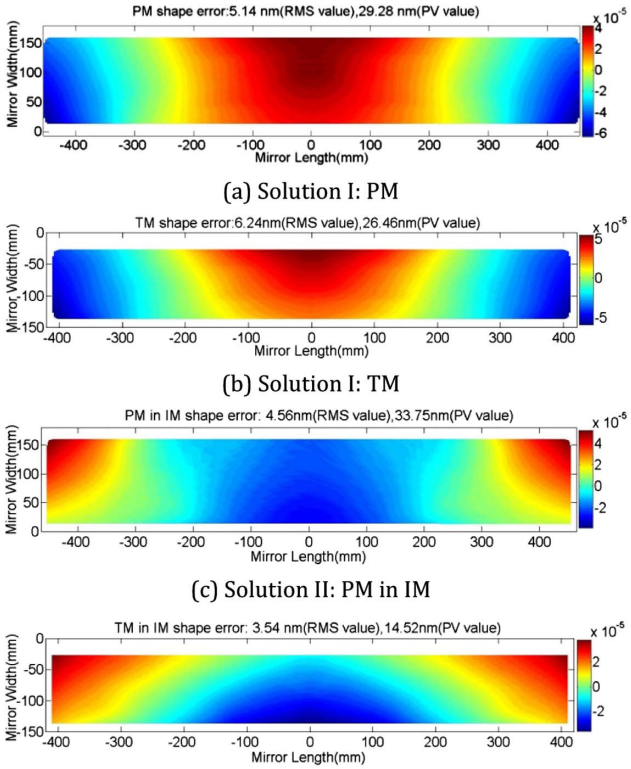

Fig. 13. Mirror shape error pseudo-color images.

Combined with opto-mechanics support structure, the PM and TM shape error values (RMS) are 5.14 nm and 6.24 nm in solution I, respectively. Remarkably, in solution II, the PM and TM working region of IM shape error values (RMS) are 4.56 nm and 3.54 nm, respectively, as shown in Table 8. Solution II has a better performance compared to solution I. The two solutions' mirror shape error pseudo-color images are shown in Fig. 13.

In terms of opto-mechanics performance, based on previous analysis, the mirror light–weight ratio is larger in solution II than in solution I. Furthermore, the opto-mechanical structure member is less in solution II than in solution I. The calculation results (shown in Table 8) show that the total weight of solution I is 20.69 kg, and 17.69 kg of solution II, 13.4% lighter.

Table 8. Opto-Mechanics Performance

		Weight (kg)							Light–Weight			
Solution		Mirror	Backboard	Cone-Shaped Sheath	Flexible Unit	Total	Size (mm)	DTR	Original Weight (kg)	Remove Weight (kg)	Light–Weight Ratio	Shape Error (nm)
I	PM	7.71	1.54	0.07*3	0.14*3	20.69	907 × 147 × 70	13.13:1	26.73	7.71	71.2%	5.14
	TM	8.84	1.34	0.07*3	0.14*3		822 × 110 × 70	11.85:1	34.77	8.84	74.6%	6.24
II	PM in IM	14.4	2.26	0.07*3	0.14*3	17.92	908 × 297 × 70	13.65:1	68.42	14.43	78.9%	4.56
	TM in IM			0.07*3	0.14*3							3.54

For a space remote sensor optical system, the opto-mechanical performance plays a significant role. A well-designed optical system will have poor performance with a weak opto-mechanical structure, and an unreasonable mirror structure will also degrade system performance.

Based on the above design and analysis from multiple perspectives, compared with solution I, solution II (PM and TM are integrated on one mirror) has advantages in terms of achieving a higher light–weight ratio, better mirror shape error, lighter opto-mechanics weight, etc.

With comprehensive analysis combined with our previous work [1], the integration of the PM and TM not only brings alignment convenience (the number of alignment DOFs is reduced from 12 to 6) but also improves opto-mechanical properties in multiple perspectives.

6. CONCLUSION

In this paper, an easy-aligned off-axis three-mirror freeform telescope with a large linear FOV based on integration mirror is designed. The system design principle is illustrated in the paper first, and the optical system initial configuration based on third-order aberration is established. Then, for the application of a freeform surface, a qualitative aberration correction ability of the *x-y* polynomial surface is analyzed, where the result provides a simple, convenient, and user-friendly relationship between freeform surface term coefficients and aberrations, and the qualitative analysis results is used to guide CODE V to adjust and optimize the freeform parameters. Based on above analysis, an example of the optical system with a focal length of 1200 mm, an *F*-number of 12, and a large linear FOV of 1° × 30° is designed. The design and tolerance results show that the system has a good imaging performance.

From the point of opto-mechanics performance of the IM, the IM structure and opto-mechanics support structure are designed. According to optimization design, we analyze the system from multiple perspectives. The confirmatory design results show that the integration of the PM and TM can improve opto-mechanical properties in multiple perspectives.

REFERENCES

1. Q. Meng, W. Wang, H. Ma, and J. Dong, "Easy-aligned off-axis three-mirror system with wide field of view using freeform surface based on integration of primary and tertiary mirror," Appl. Opt. **53**, 3028–3034 (2014).
2. N. Ohgi, A. Iwasaki, T. Kawashima, and H. Inada, "Japanese hyper-multi spectral mission," in *Proceedings of IEEE Conference on Geoscience and Remote Sensing Symposium (IGARSS)* (IEEE, 2010), pp. 3756–3759.
3. J. W. Figoski, "Aligment and test results of the QuickBird telescope using ball optical system test facility," Proc. SPIE **3785**, 99–108 (1999).
4. V. K. Hariharan, N. S. Sundaram, K. S. Dayashankara, V. Lakshminarayana, A. K. Shrivastava, A. Damodaran, L. N. Gupta, P. P. Ganeshan, M. Velayudhan, B. V. Rao, N. D. Ghatpande, and T. L. Danabalan, "Assembly, integration and testing of Cartosat-1," in *Proceedings of IEEE Conference on Electromagnetic Interference and Compatibility (INCEMIC)* (IEEE, 2006), pp. 60–66.
5. G. Baer, J. Schindler, C. Pruss, and W. Osten, "Correction of misalignment introduced aberration in non-null test measurements of free-form surfaces," J. Eur. Opt. Soc. **8**, 13074 (2013).
6. K. P. Thompson and J. P. Rolland, "Freeform optical surface a revolution in imaging optical design," Opt. Photon. News **23**(6), 30–35 (2012).
7. J. M. Rodgers, "Unobscured mirror designs," Proc. SPIE **4832**, 33–60 (2002).
8. L. G. Cook, "Three mirror anastigmatic optical system," U.S. patent 4265510 (5 May 1981).
9. W. B. Wetherell and D. A. Womble, "All-reflective three element objective," U.S. patent 4240707 (23 December 1980).
10. L. G. Cook, "Reflective optical triplet having a real entrance pupil," U.S. patent 4733955 (29 March 1988).
11. L. W. Fritz, "Commercial earth observation satellites," Int. Arch. Photogramm. Remote Sens. **31**, 273–282 (1996).
12. Q. Meng, J. Dong, D. Wang, and W. Liang, "Off-axis two-mirror system with wide field of view based on diffractive mirror," J. Opt. Soc. Korea **19**, 604–613 (2015).
13. M. Beier, J. Hartung, T. Peschel, C. Damm, A. Gebhardt, S. Scheiding, D. Stumpf, U. D. Zeitner, S. Risse, R. Eberhardt, and A. Tünnermann, "Development, fabrication, and testing of an anamorphic imaging snap-together freeform telescope," Appl. Opt. **54**, 3530–3542 (2015).
14. M. Beier, J. Hartung, J. Kinast, A. Gebhardt, F. Burmeister, U. D. Zeitner, S. Risse, R. Eberhardt, and A. Tünnermann, "Fabrication of metal mirror modules for snap-together VIS telescopes," Proc. SPIE **9633**, 963313 (2015).
15. T. Yang, J. Zhu, X. Wu, and G. Jin, "Direct design of freeform surfaces and freeform imaging systems with a point-by-point three dimensional construction-iteration method," Opt. Express **23**, 10233–10246 (2015).
16. J. Zhu, W. Hou, X. Zhang, and G. Jin, "Design of a low F-number freeform off-axis three-mirror system with rectangular field-of-view," J. Opt. **17**, 015605 (2015).
17. H. Gross, "Advanced lens design," http://www.iap.uni-jena.de/Institute/Teaching/Archive.html.
18. T. Peschel, C. Damm, S. Scheiding, M. Beier, S. Risse, S. Nikolov, W. Holota, S. Weiß, and P. Bartsch, "Anamorphotic telescope for earth observation in the mid-infrared range," in *Proceedings of International Conference on Space Optics (ICSO)* (2014).
19. I. J. Saunders, L. Ploeg, M. Dorrepaal, and B. V. Venrooij, "Fabrication and metrology of freeform aluminum mirrors for the SCUBA-2 instrument," Proc. SPIE **5869**, 586905 (2005).
20. W. Hou, J. Zhu, T. Yang, and G. Jin, "Construction method through forward and reverse ray tracing for a design of ultra-wide linear field-of-view off-axis freeform imaging systems," J. Opt. **17**, 055603 (2015).
21. T. Yang, J. Zhu, and G. Jin, "Compact freeform off-axis three-mirror imaging system based on the integration of primary and tertiary mirrors on one single surface," Chin. Opt. Lett. **14**, 060801 (2016).
22. J. P. McGuire, Jr., "A fast, four-mirror, free-form, wide field of view, telecentric telescope," in *Renewable Energy and the Environment*, OSA Technical Digest (online) (Optical Society of America, 2013), paper FT3B.6.
23. X. Zhang, L. Zheng, X. He, L. Wang, F. Zhang, S. Yu, G. Shi, B. Zhang, Q. Liu, and T. Wang, "Design and fabrication of imaging optical systems with freeform surfaces," Proc. SPIE **8486**, 848607 (2012).
24. Synopsys Inc., Code V Reference Manual (2012).
25. D. A. Atchison, D. H. Scott, and M. J. Cox, "Mathematical treatment of ocular aberrations: a user's guide," in *Vision Science and Its Applications*, V. Lakshminarayanan, ed. (Optical Society of America, 2000), Vol. **35**, pp. 110–130.